The Journal of Anatomical Sciences
Email: journalofanatomicalsciences@gmail.com

J. Anat Sci 17(1) Mar

Submitted: November 12th, 2025
Revised: January 22nd, 2026
Accepted: February 10th, 2026

The Forensic Spleen and Lungs: Comparing the Histo-taphonomy of Porcine Structures in Postmortem Interval Estimation

*Nandi, M.E., Okpam, E.O., Iyam U.C., Tangban, C.N., Imasa, E.U., Ojo, I., Usang, B. G., Oko V.O.

Department of Anatomy and Forensic Anthropology, Faculty of Basic Medical Sciences, University of Cross River State, Nigeria.

***Corresponding Author:**
Email: m.enandi@unicross.edu.ng; Tel: +2347032867876

ABSTRACT

Accurate determination of the postmortem interval (PMI) remains problematic in forensic investigations due to the complexity of biological and environmental factors that influence tissue decomposition. This study conducted a comparative histotaphonomic analysis of splenic and pulmonary tissues in porcine models to evaluate their reliability as biological indicators for PMI estimation. Sixteen (16) healthy domestic pigs (*Sus scrofa domestica*) were humanely euthanized, and spleen and lung tissues were harvested and maintained under specified conditions to decompose over five days. Tissue samples were collected at 0, 2, 6, and 10 hours postmortem on Day 1, and daily from Days 2 to 5, fixed in Bouin's solution, and stained using histological assessment performed using Hematoxylin–Eosin (H&E) and Masson's Trichrome (MT). At 0–2 hours postmortem, the spleen showed intact white and red pulps, while the lungs showed well-defined alveolar sacs and bronchioles. Early autolytic changes, including nuclear shrinkage and mild structural disorganization, appeared by 6–10 hours. By Day 2, both organs demonstrated marked cellular degradation, with the spleen showing nuclear loss and matrix disorganization and the lungs exhibiting alveolar collapse and epithelial pyknosis. MT staining revealed progressive collagen degradation and connective tissue atrophy from Day 3 onward, with more pronounced changes in the lungs. By Day 5, both organs showed advanced decomposition with complete architectural collapse. Overall, the lungs decomposed faster than the spleen, suggesting greater usefulness of pulmonary tissues for early PMI estimation, whereas splenic tissues serve as a more reliable indicator during later stages of decomposition.

Keywords: histotaphonomy, postmortem interval, spleen, lungs, decomposition

INTRODUCTION

Decomposition is an unavoidable biological phenomenon that begins immediately after death. At first, deterioration is not externally apparent because breakdown initiates at the cellular level. Gradually, these microscopic alterations develop into visible postmortem changes[1]. This process persists beyond the dry-remains stage, as skeletal tissues continue to degrade, albeit at a considerably slower rate. Ultimately, decomposition supports the redistribution of energy and nutrients back into the surrounding ecosystem[1, 2].

The postmortem interval (PMI) is defined as the duration between death and the discovery of the body. Information obtained from PMI estimation, together with other forms of evidence, assists in identifying the deceased and guiding forensic investigations[3,4,5]. Various approaches are employed to estimate PMI, including forensic pathology, entomology, ocular assessment, biochemical and microbiological analyses, taphonomic methods, and forensic anthropological decomposition scoring systems[4, 6, 7]. Nevertheless, these techniques exhibit limitations and vary in accuracy in practical application.

Estimating PMI is a multifaceted task influenced by numerous internal and external variables, as well as environmental conditions such as temperature[4,8,9], humidity, rainfall, and soil characteristics[3,4]. Biological contributors, including scavenging, predation, microbial action, and enzymatic activity[3, 4, 10], also significantly affect decomposition. PMI assessment typically relies on external examination, evaluating indicators such as body cooling, livor mortis, rigor mortis, autolysis, and putrefaction[11,12]. As the time since death increases, determining PMI with precision becomes progressively more challenging[12].

Some authors categorize the postmortem period into early and late phases[13-16]. The early phase is commonly assessed through physical examination of the body[13,15,17,18] and concludes when soft tissue breakdown begins[14], usually within the first 24 hours following death[13;15]. The late postmortem phase extends from days to months or even years after death; during this stage, narrowing PMI becomes increasingly unreliable[16], as corpse examination, decomposition evaluation, skeletal radiometric dating, and entomological analyses are heavily affected by individual and environmental variability[12, 13, 15, 17].

In recent years, several laboratory-based techniques have been introduced to enhance PMI estimation, complementing conventional physico-chemical indicators (body cooling, lividity, rigor mortis), chemical markers (autolysis), microbiological processes (putrefaction), entomological evidence, radiocarbon dating, and botanical parameters[11,15,16,19].

Histotaphonomy is an interdisciplinary field encompassing forensic science, physical anthropology, and palaeoenvironmental research, focusing on the microstructural assessment and interpretation of taphonomic changes in human remains[20; 21; 22]. Histology characterizes normal cellular and tissue architecture, whereas histopathology specializes in identifying pathological changes. In both disciplines, samples obtained from living or deceased organisms are preserved in formaldehyde (commonly 10% neutral buffered formalin), processed through graded alcohol concentrations (70%–100%), embedded in paraffin, sectioned, mounted on slides, and stained to enable microscopic visualization of cellular and tissue differentiation[23].

Within forensic science, histological and histopathological analyses support macroscopic observations made during clinical examination, scene investigation, or autopsy[24-26]. The use of hematoxylin–eosin staining and specialized techniques such as immunohistochemistry has broad forensic applications, including assessment of sample type, lesion age and vitality, and determination of cause of death[25]. As widely available, efficient, and cost-effective methodologies, histological techniques are recognized as essential tools in forensic investigations[25-27].

There is limited information on histotaphonomic studies comparing multiple organs. Moreover, there is a scarcity of data on the degradation patterns of spleen and lung tissue, and a lack of standardized histological markers for PMI estimation. Therefore, there is a need for organ-specific histological timelines for forensic application. This study seeks to address this knowledge gap through the examination and comparison of the histotaphonomic changes in the spleen and lung tissues of porcine models, providing valuable insights into PMI estimation.

MATERIALS AND METHODS

Ethical approval

Before initiating the study, ethical clearance was obtained from the Faculty of Basic Medical Sciences Research and Ethics Committee (FBMSREC) of the University of Cross River State, Okuku Campus, Nigeria. Approval was granted under reference number FBMS/REC/2024/017 and formally communicated to the principal investigator. All experimental protocols adhered strictly to institutional regulations and ethical guidelines governing the humane use of animals for research purposes.

Experimental animals and handling

Sixteen (16) domestic pigs (*Sus scrofa domestica*), each weighing between 34 and 35 kg, were utilized in this investigation. The animals were procured from a local piggery located less than 2 km from the research facility and transported to the Department of Anatomy and Forensic Anthropology Research Facility (DAFARF) at the University of Cross River State, Okuku Campus. Prior to acquisition, all pigs were clinically evaluated and certified healthy by a licensed veterinary professional. Due to the proximity of the piggery to the research facility, no acclimatization period was required. Upon arrival from the piggery, all pigs were immediately humanely euthanized simultaneously using sharp force trauma directed through the axilla into the trachea at exactly 1:14 pm, ensuring rapid loss of consciousness and death confirmation. Immediately after death, the carcasses were eviscerated, and the spleen and lungs were carefully excised and placed on cemented platforms within the research house under controlled environmental conditions for decomposition assessment.

Experimental design

The experiment was conducted at the Department of Anatomy and Forensic Anthropology Research Facility (DAFARF) under controlled indoor conditions. Sixteen domestic pigs (*Sus scrofa domestica*) of comparable body weight served as experimental models. The entire experimental period spanned five (5) days, during which splenic and pulmonary tissue samples were collected at regular postmortem intervals. Following euthanasia and confirmation of death at 1:14 pm, all carcasses were eviscerated, and the spleens and lungs were arranged 2 meters apart to minimize cross-contamination and ensure even exposure to environmental factors. Sampling intervals were systematically maintained to document histotaphonomic changes relevant to postmortem interval (PMI) estimation.

Tissue sampling

At exactly 1:14 pm, immediately after death confirmation, the first spleen and lung samples were collected and designated as control samples (0 hour PMI). Subsequent samples were collected at 2 hours,

6 hours, and 10 hours postmortem on the first day. From Day 2 to Day 5, tissue sampling occurred once daily (evening). All tissue samples were promptly labeled and fixed in appropriate fixatives to prevent further autolysis prior to histological processing.

Tissue processing and histological analysis

Immediately after collection, spleen and lung specimens were fixed in Bouin's solution consisting of 75% picric acid, 5% glacial acetic acid, and 25% buffered 40% formalin. Following six (6) hours of fixation, tissues were transferred into 70% ethanol for preservation before processing.

Samples were dehydrated through graded ethanol concentrations, cleared with xylene, and infiltrated with molten paraffin wax to ensure adequate tissue impregnation. The tissues were embedded in paraffin blocks, sectioned at 5 µm thickness using a rotary microtome, and mounted onto clean glass slides.

Routine histological staining was carried out with Hematoxylin and Eosin (H&E) to assess general tissue structure[29], while Masson's Trichrome (MT) was employed to evaluate collagen fibers and connective tissue organization[30]. Prepared slides were examined using a light microscope, and photomicrographs were captured for documentation. Histotaphonomic changes, including tissue architecture disruption, cellular degradation, vascular collapse, and collagen breakdown, were analyzed comparatively between the spleen and lung tissues to estimate PMI reliability.

RESULTS

Comparative histological observations of the spleen and lungs stained with H&E

The 0-hour postmortem (control) spleen tissue (Figure 1) showed a normal splenic architecture characterized by a well-preserved central vein (Cv), distinctly identifiable white pulp (Wp) and red pulp (Rp) areas, intact marginal zone (Mz), and abundant red blood cells (Rc) within the splenic cords, indicating no observable postmortem effect. Similarly, the 0-hour lung tissue (Figure 2) displayed a normal respiratory histoarchitecture consisting of well-defined alveolar sacs (As) lined by intact alveolar cells (Asc), terminal bronchioles (Tb) with well-lined bronchial epithelium (Be), visible smooth muscle (Sm), and numerous pneumocytes (Pn) within the respiratory matrix — also showing no observable effect.

At 2 hours postmortem, both spleen (Figure 3) and lung (Figure 4) tissues maintained their normal histological organization. The spleen showed preserved central vein, white pulp, and red pulp. At the same time, the lung retained well-defined alveolar sacs, blood vessels, and bronchiolar lining epithelium, confirming no visible histotaphonomic alterations within the first 2 hours after death.

By 6 hours, PMI, early autolytic changes were observed. The spleen tissue (Figure 5) showed slight abnormalities in its general architecture with loss of some cellular nuclei within the red pulp area, indicating the onset of early postmortem changes. The lung tissue at the same interval (Figure 6) showed gradual degradation of alveolar sacs, mild vacuolation, and early nuclear distortion within the respiratory matrix, signifying a mild histotaphonomic effect in both tissues.

At 10 hours, PMI, more distinct decomposition changes became apparent. The spleen (Figure 7) displayed disoriented splenic architecture with visible shrinking nuclei (Sn) within the matrix and slightly disrupted white and red pulp regions, indicating a mild histotaphonomic effect. The lung tissue (Figure 8), however, exhibited a moderate effect, showing degraded alveolar sacs, shrunken nuclei, and structural distortion of bronchioles (B) and alveolar walls, suggesting that the lung was decomposing slightly faster than the spleen at this stage.

By Day 2 evening (30 hours PMI), both organs showed marked histological deterioration. The spleen (Figure 9) demonstrated disoriented splenic architecture with widespread shrinking nuclei within the splenic matrix, indicative of severe histotaphonomic change corresponding to the bloat stage of decomposition. The lung tissue (Figure 10) revealed widespread degradation of alveolar sacs, with shrinking (Sn) and anucleated (Ac) cells appearing prominently, reflecting severe damage and progression to the active decay stage.

At Day 3 evening (54 hours PMI), the spleen (Figure 11) showed further disorganization of splenic tissue and a wide presentation of anucleated cells (Ac) within the matrix, signifying severe cellular degradation. Similarly, the lung (Figure 12) demonstrated distorted respiratory histoarchitecture with extensive anucleation and complete loss of alveolar definition, indicating advanced histotaphonomic alteration.

By Day 4 evening (78 hours PMI), both spleen and lung tissues exhibited extensive structural collapse. The spleen (Figure 13) showed complete disorientation with widespread anucleated cells (Ac) and total loss of tissue definition. In contrast, the lung (Figure 14) demonstrated extensive anucleation and collapse of alveolar integrity, indicating advanced decay and severe histotaphonomic effect in both tissues.

By Day 5 evening (102 hours PMI), both tissues were in an advanced decay stage. The spleen (Figure 15) showed severe disorientation with widespread anucleation and total loss of splenic microarchitecture, while the lung (Figure 16) displayed complete distortion of respiratory tissue, collapsed alveolar sacs, and extensive cellular anucleation, signifying terminal tissue breakdown.

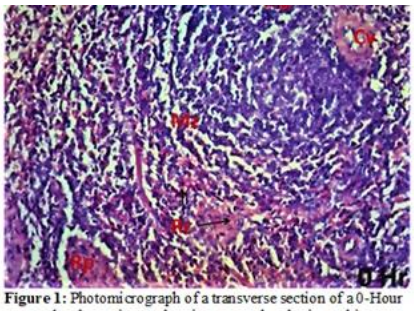

Figure 1: Photomicrograph of a transverse section of a 0-Hour exposed spleen tissue showing normal splenic architecture having central vein (Cv), white pulp (Wp), marginal zone (Mz), red blood cell (Rc), and red pulp (Rp) (H&E x100).

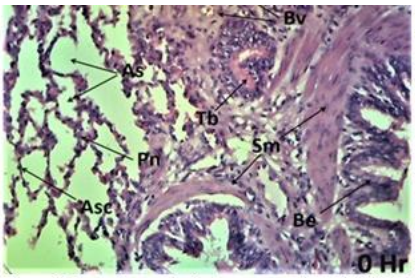

Figure 2: Photomicrograph of a transverse section of a (0-Hour) exposed lung tissue demonstrating normal respiratory histostructure having alveolar sacs (As) with well-lined alveolar cells (Asc), blood vessels (Bv), terminal bronchioles (Tb) with well-lined bronchial epithelium (Be), smooth muscle (Sm), and wide spread Pneumocytes (Pn) within the respiratory matrix (H&E x100).

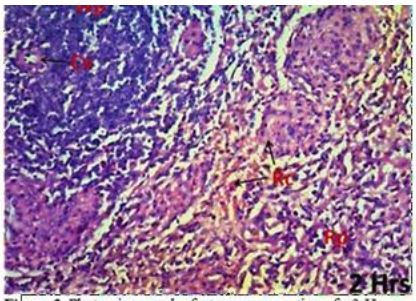

Figure 3: Photomicrograph of a transverse section of a 2-Hours exposed spleen tissue showing normal splenic architecture having central vein (Cv), white pulp (Wp), red blood cell (Rc), and red pulp (Rp) (H&E x100).

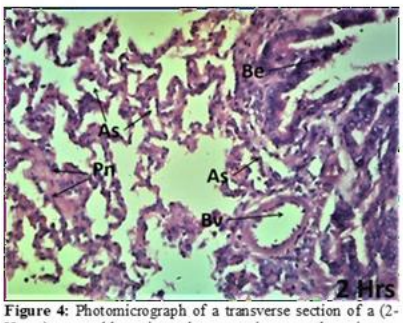

Figure 4: Photomicrograph of a transverse section of a (2-Hours) exposed lung tissue demonstrating normal respiratory histostructure having alveolar sacs (As), blood vessels (Bv), terminal bronchioles with well-lined bronchial epithelium (Be), and wide spread Pneumocytes (Pn) within the respiratory matrix (H&E x100).

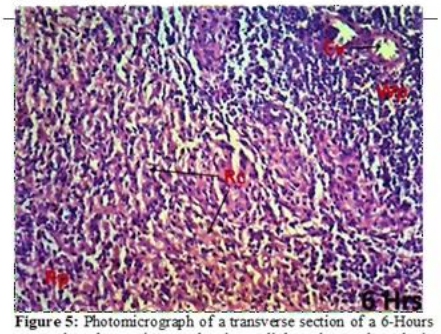

Figure 5: Photomicrograph of a transverse section of a 6-Hours exposed spleen tissue showing slight abnormal splenic architecture having central vein (Cv), white pulp (Wp), red blood cells (Rc), and the red pulp (Rp) area with loss cell nuclei (H&E x100).

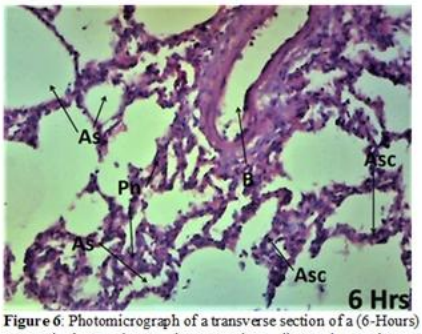

Figure 6: Photomicrograph of a transverse section of a (6-Hours) exposed lung tissue demonstrating distorted respiratory histostructure having gradual degrading of alveolar sacs (As) with alveolar cells (Asc), bronchiole (B), and Pneumocytes (Pn) within the respiratory matrix (H&E x100).

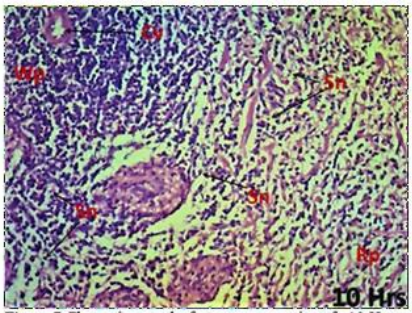

Figure 7: Photomicrograph of a transverse section of a 10-Hours exposed spleen tissue showing disoriented splenic architecture having central vein (Cv), white pulp (Wp), red pulp (Rp), and shrinking nuclei (Sn) within the matrix (H&E x100).

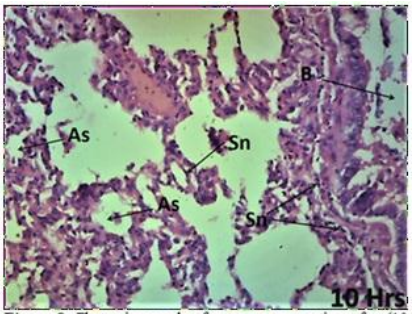

Figure 8: Photomicrograph of a transverse section of a (10-Hours) exposed lung tissue demonstrating distorted respiratory histostructure having degraded alveolar sacs (As) with shrinking nuclei (Sn) and bronchiole (B) within the respiratory matrix (H&E x100).

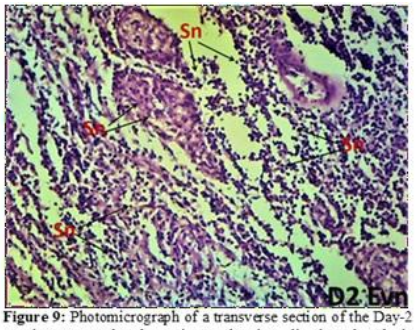

Figure 9: Photomicrograph of a transverse section of the Day-2 evening exposed spleen tissue showing disoriented splenic architecture with widely spread shrinking nuclei (Sn) within the splenic matrix (H&E x100).

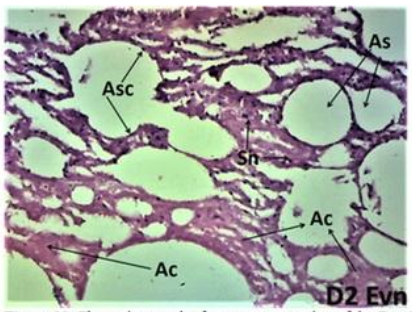

Figure 10: Photomicrograph of a transverse section of the Day-2 evening (30hrs) exposed lung tissue demonstrating distorted respiratory histo-structure having wide presentation of degraded alveolar sacs (As) with shrinking nuclei (Sn) and anucleated nuclei (Ac) within the respiratory matrix (H&E x100).

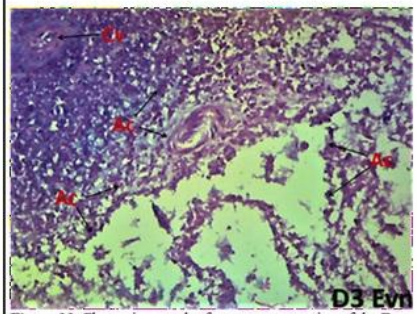

Figure 11: Photomicrograph of a transverse section of the Day-3 evening exposed spleen tissue showing disoriented splenic architecture having central vein and wide presentation of anucleated cells (Ac) within the splenic matrix (H&E x100).

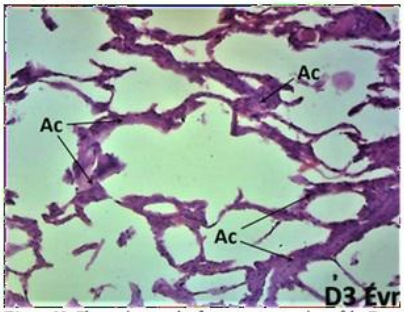

Figure 12: Photomicrograph of a transverse section of the Day-3 evening (54 hrs) exposed lung tissue demonstrating distorted respiratory histostructure having wide presentation of anucleated nuclei (Ac) within the respiratory matrix (H&E

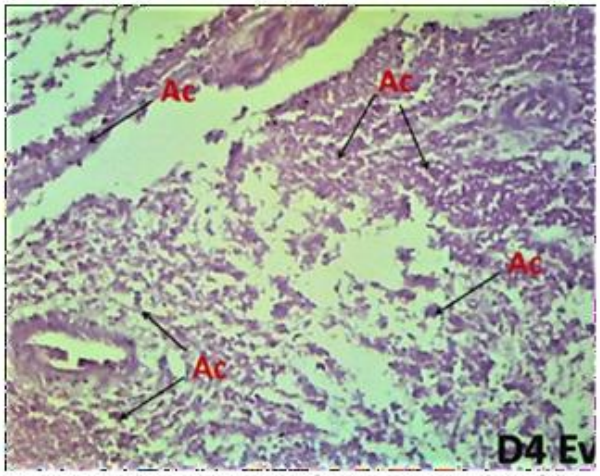

Figure 13: Photomicrograph of a transverse section of the Day-4 evening exposed spleen tissue showing disoriented splenic architecture with widely spread anucleated cells (Ac) within the splenic matrix (H&E x100).

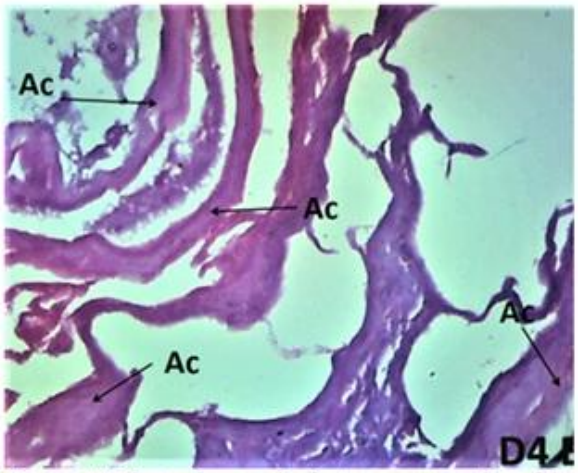

Figure 14: Photomicrograph of a transverse section of the Day-4 evening (78hrs) exposed lung tissue demonstrating distorted respiratory histostructure having wide presentation of anucleated nuclei (Ac) within the respiratory matrix (H&E x100).

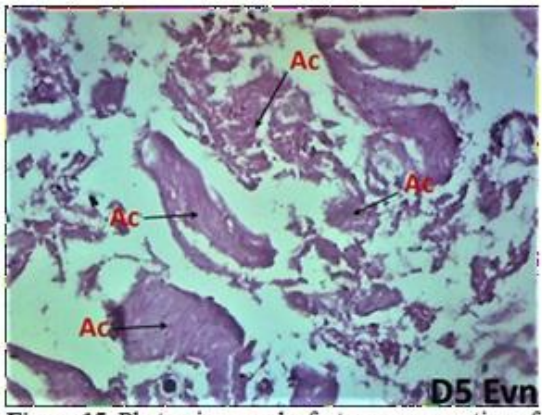

Figure 15: Photomicrograph of a transverse section of the Day-5 evening exposed spleen tissue showing disoriented splenic architecture having wide presentation of anucleated cells (Ac) within the splenic matrix (H&E x100).

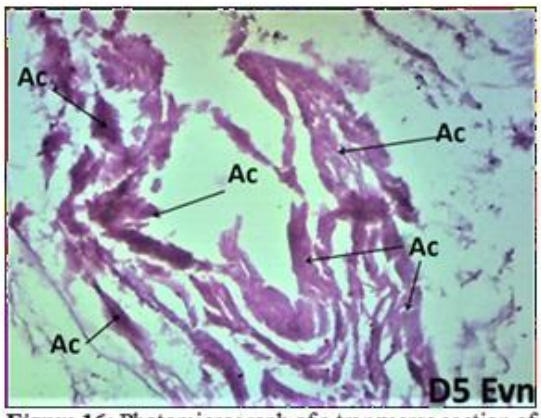

Figure 16: Photomicrograph of a transverse section of the Day-5 evening (102 hrs) exposed lung tissue demonstrating distorted respiratory histo-structure having wide presentation of anucleated nuclei (Ac) within the respiratory matrix (H&E x100).

Comparative histological observations of the spleen and lung stained with Masson's trichrome

This result revealed that at 0-hour PMI, both the spleen and lung tissues exhibited normal connective tissue integrity. The spleen showed a well-organized splenic interstitium with areas of collagen deposition (red arrow), central vein (Cv), and tubercle (Tb) (Figure 17). Similarly, the lung tissue at 0 hours presented normal connective tissue within the respiratory parenchyma, marked by an intense collagen deposit (red arrow) (Figure 18). These observations represented the baseline structural integrity of both tissues at the fresh stage.

At 2 hours PMI, the spleen maintained normal connective tissue features within the splenic interstitium, still showing distinct collagen deposits (red arrow) and evident red blood cells (Rbc) within the tissue matrix (Figure 19). The lung at this stage retained normal tissue organization with wide and intense collagen deposition within the connective framework (Figure 20). Both organs showed minimal alteration, characteristic of the early postmortem phase.

By 6 hours PMI, the spleen continued to exhibit normal connective tissue distribution with visible collagen deposits (red arrow) within the interstitium (Figure 21). The lung tissue maintained its respiratory architecture with prominent collagen deposits (red arrow) (Figure 22), suggesting the early onset of

biochemical degradation with no major histological distortion in both organs.

At 10 hours PMI, the spleen still presented a fairly preserved connective tissue network within the splenic interstitium with mild areas of collagen deposition (red arrow) (Figure 23). However, the lung tissue began to show less intense collagen deposits (red arrow) (Figure 24), indicating the commencement of connective tissue breakdown and early structural weakening as decomposition progressed toward the bloat stage.

By day 2 evening (30 hours PMI), the spleen maintained a normal connective tissue arrangement with moderate collagen deposition (Figure 25). Conversely, the lung exhibited widespread collagen deposits (red arrow) within the respiratory parenchyma (Figure 26), suggesting an ongoing histological response to progressive decay, with the tissue now approaching the active decay stage.

At day 3 evening (54 hours PMI), the spleen showed diminished collagen presence with observable fibrous deposits within the splenic interstitium (Figure 27). The lung tissue demonstrated decreased collagen intensity and disorganized connective tissue presentation (red arrow) (Figure 28), marking notable structural alteration consistent with the advanced decomposition phase.

By day 4 evening (78 hours PMI), the spleen presented increased areas of atrophied fibrous deposits within the interstitium (Figure 29), indicating substantial tissue degradation. In contrast, the lung tissue displayed severely altered architecture with the absence of visible collagen deposits (Figure 30), confirming advanced connective tissue breakdown and loss of structural integrity.

Finally, by day 5 evening (102 hours PMI), the spleen demonstrated extensive fibrous atrophy and tissue disorganization within the interstitium (Figure 31). At the same time, the lung exhibited a complete loss of collagen with a distorted connective matrix (Figure 32). Both tissues exhibited severe histotaphonomic alterations characteristic of the advanced decay stage, with the lung showing greater susceptibility to connective tissue degradation than the spleen.

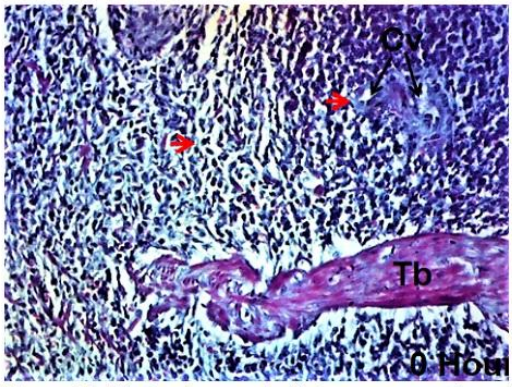

Figure 17: Photomicrograph of a transverse section of a 0 Hour exposed spleen presenting a normal connective tissue deposit within the splenic interstitium with areas of collagen deposit (red arrow), central vein (Cv) and tubercle (Tb) (MT x100).

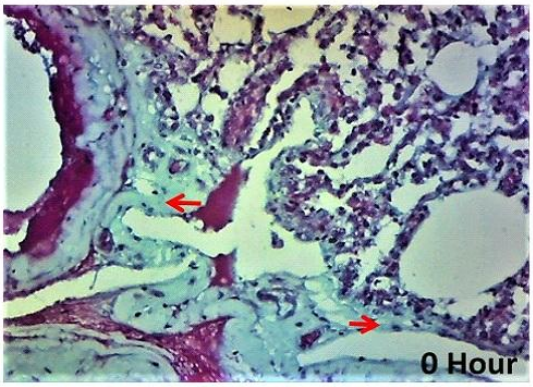

Figure 18: Photomicrograph of a transverse section of a 0-Hour exposed Lung tissue presenting a normal connective tissue deposit within the respiratory tissue with wide intense collagen deposit (red arrow) (MT x100).

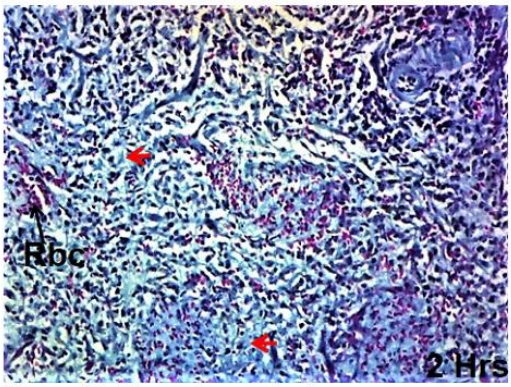

Figure 19: Photomicrograph of a transverse section of a 2 Hours exposed heart presenting a normal connective tissue presence within the cardiac tissues with areas of collagen and fibrous tissue deposit (yellow arrow) (MT x100).

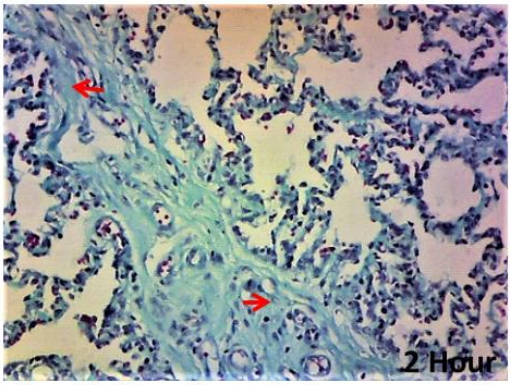

Figure 20: Photomicrograph of a transverse section of a 2-Hour exposed Lung tissue presenting a normal connective tissue deposit within the respiratory tissue with wide intense collagen deposit (red arrow) (MT x100).

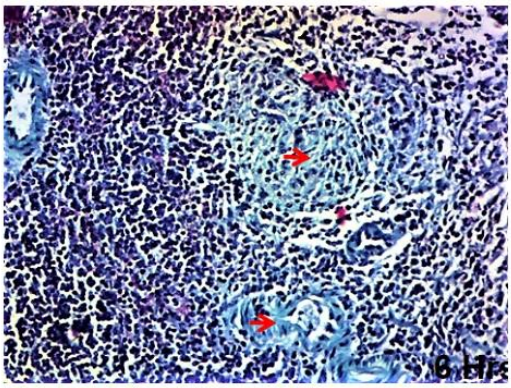

Figure 21: Photomicrograph of a transverse section of a 6 Hours exposed spleen presenting a normal connective tissue deposit within the splenic interstitium with areas of collagen deposit (red arrow) (MT x100).

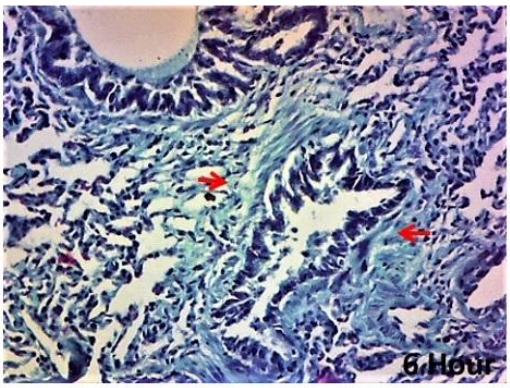

Figure 22: Photomicrograph of a transverse section of a 6-Hour exposed Lung tissue presenting a normal connective tissue deposit within the respiratory tissue with wide intense collagen deposit (red arrow) (MT x100).

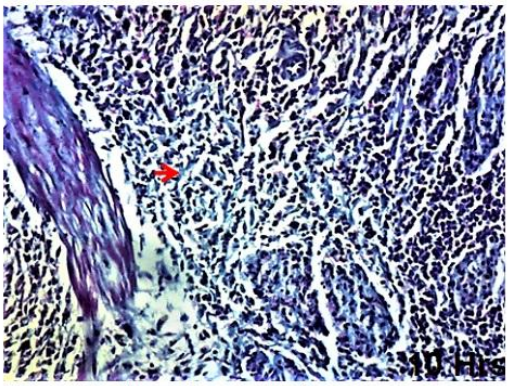

Figure 23: Photomicrograph of a transverse section of a 10 Hours exposed spleen presenting a normal connective tissue deposit within the splenic interstitium with areas of collagen deposit (red arrow) (MT x100).

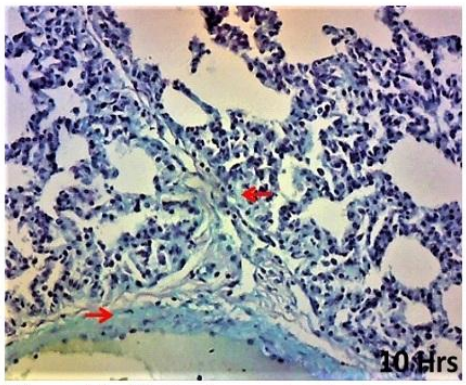

Figure 24: Photomicrograph of a transverse section of a 10-Hour exposed Lung tissue presenting a normal connective tissue deposit within the respiratory tissue with less intense collagen deposit (red arrow) (MT x100).

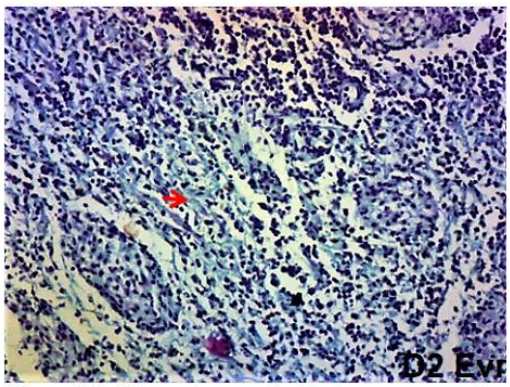

Figure 25: Photomicrograph of a transverse section of a day 2 evening exposed spleen presenting a normal connective tissue deposit within the splenic interstitium with areas of collagen deposit (red arrow) (MT x100)

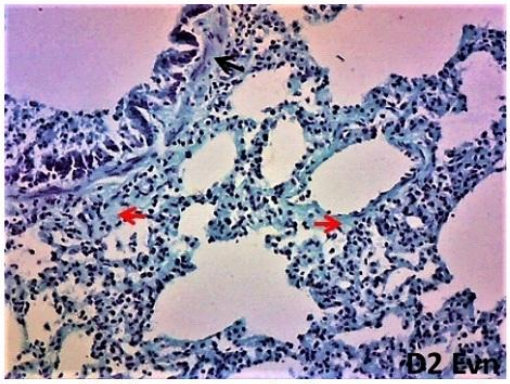

Figure 26: Photomicrograph of a transverse section of a Day 2 evening 30-Hours exposed Lung tissue presenting a normal connective tissue deposit within the respiratory tissue with wide spread collagen deposit (red arrow) (MT x100).

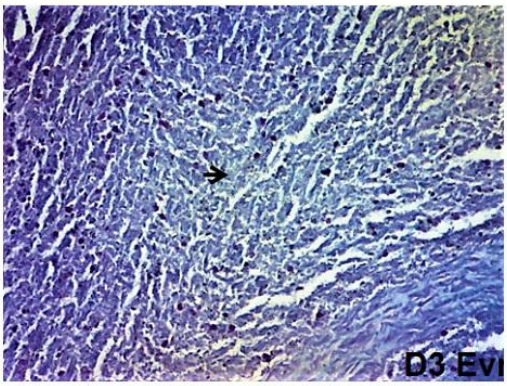

Figure 27: Photomicrograph of a transverse section of a day 3 evening exposed spleen presenting connective tissue deposit within the splenic interstitium with no obvious collagen deposit and areas of fibrous deposit (MT x100).

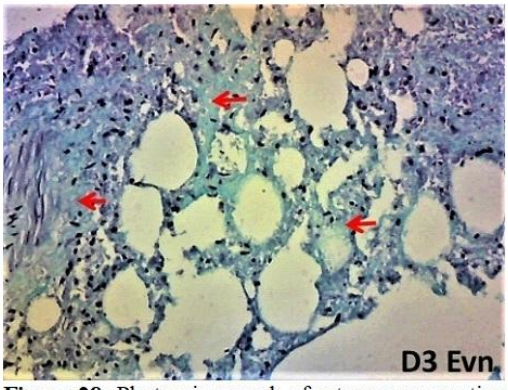

Figure 28: Photomicrograph of a transverse section of a Day 3 Evening 54-Hours exposed Lung illustrating the altered presentation of connective tissue within the respiratory tissue with decreased collagen deposit (red arrow) (MT x100).

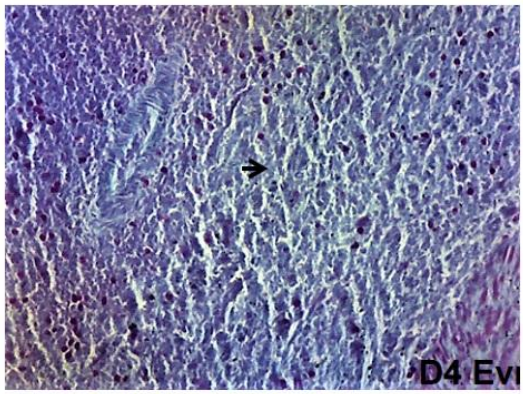

Figure 29: Photomicrograph of a transverse section of a day 4 evening exposed spleen demonstrating connective tissue within the splenic interstitium with increase areas of atrophied fibrous deposit (MT x100).

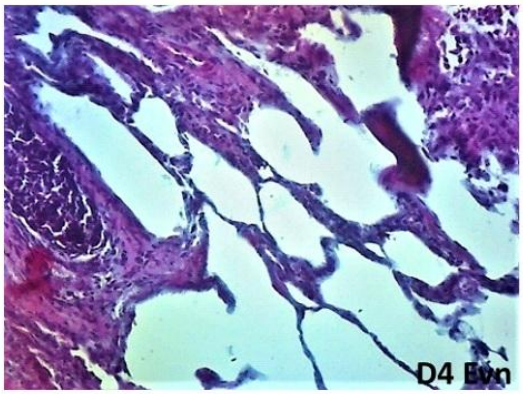

Figure 30: Photomicrograph of a transverse section of a Day 4 evening 78-Hours exposed Lung illustrating the altered presentation of connective tissue within the respiratory tissue with no obvious collagen deposit (MT x100).

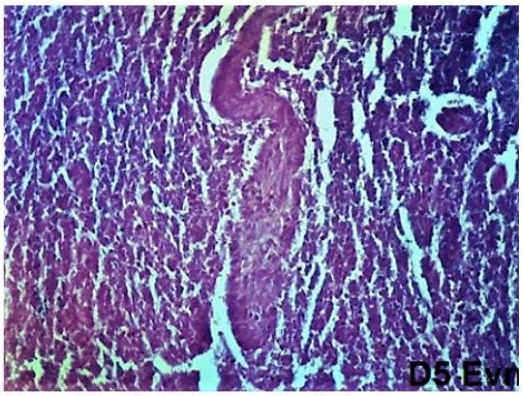

Figure 31: Photomicrograph of a transverse section of a day 5 evening exposed spleen demonstrating connective tissue within the splenic interstitium with increase areas of atrophied fibrous deposit (MT x100).

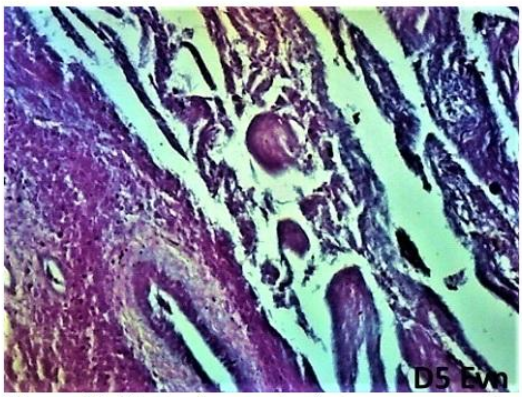

Figure 32: Photomicrograph of a transverse section of a Day 5 evening 102-Hours exposed Lung illustrating the altered presentation of connective tissue within the respiratory tissue with no obvious collagen deposit (MT x100).

DISCUSSION

Accurate estimation of the postmortem interval (PMI) remains a fundamental objective in forensic investigations, and the microscopic evaluation of organ-specific decomposition patterns has gained increasing attention as a complementary approach to traditional methods. Internal organs such as the spleen and lungs are particularly informative because of their high cellularity, vascularity, and connective tissue content, which make them susceptible to predictable changes caused by autolysis and putrefaction following death[31,32].

In the present study, both the spleen and lungs maintained preserved histoarchitecture within the first 0–2 hours postmortem, consistent with the concept that early PMI is dominated by residual cellular metabolism and delayed autolysis in well-perfused tissues[33]. The preserved splenic red and white pulps and intact pulmonary alveolar architecture observed during this interval align with baseline porcine histology reported by Palić *et al.*[34] and with experimental postmortem models in large mammals demonstrating minimal microscopic alteration during the immediate postmortem phase[35].

Between 6 and 10 hours postmortem, both organs began to exhibit early degenerative changes, including nuclear shrinkage, loss of cellular detail, and mild architectural disorganization. These findings are consistent with the onset of autolysis, driven by lysosomal enzyme release and progressive membrane failure following circulatory arrest, as seen in studies by Sluis *et al.*[36] and Almulhim[37]. The earlier and more pronounced alveolar distortion observed in the lung supports previous reports by Pittner *et al.*[35] and Zissler *et al.*[32] that pulmonary tissue decomposes more

rapidly due to its high oxygen exposure, thin alveolar septa, and microbial accessibility via the airways.

By approximately 30 hours postmortem, corresponding to the bloat and early active decay stages, marked histological deterioration was evident in both tissues. The spleen demonstrated extensive nuclear loss and disruption of pulpal organization, while the lungs showed fragmentation of alveolar septa and widespread karyolysis. Similar patterns of mid-stage histotaphonomic change have been documented in controlled human and animal studies, in which progressive cellular disintegration and loss of tissue cohesion have been identified as reliable indicators of intermediate PMI[7,32,35].

Masson's trichrome staining further elucidated the differential breakdown of connective tissue components. During early postmortem intervals, preserved collagen distribution reflected the relative resistance of extracellular matrix proteins to immediate enzymatic degradation, as previously described by Jellinghaus *et al.*[38]. However, by Days 3–4, both organs exhibited fragmented and atrophied collagen fibers, consistent with advanced autolysis and microbial proteolysis. The more rapid loss of collagen integrity in lung tissue supports earlier observations that pulmonary connective tissue degrades faster than that of encapsulated organs such as the spleen[12,31].

At Day 5 postmortem, both spleen and lung tissues demonstrated severe histoarchitectural collapse, characterized by extensive anucleation, connective tissue atrophy, and complete loss of normal microanatomy. These features correspond to the terminal stage of decomposition, during which liquefaction and structural collapse dominate soft tissue morphology[33,39].

CONCLUSION

This study concludes that histological evaluation of the spleen and lungs provides a dependable approach for determining the postmortem interval (PMI) based on their unique and time-dependent patterns of cellular and connective tissue degradation. The spleen, with its denser fibrous structure, decomposes more slowly than the lungs; therefore, it is a better indicator for later PMI estimation, whereas the lungs are more useful for detecting early postmortem changes.

REFERENCES

1. Tibbett M, Carter DO. Research in forensic taphonomy: A soil-based perspective. In: Ritz K, Dawson L, Miller D, editors. Criminal and Environmental Soil Forensics. Bradford: Springer Science & Business Media; 2009. p. 317–331.
2. Fenoglio S, Bo T, Cammarata M, Malacarne G, Del Frate G. Contribution of macro- and micro-consumers to the decomposition of fish carcasses in low-order streams: An experimental study. Hydrobiologia. 2010;637(1):219–228.
3. Boaks A, Siwek D, Mortazavi F. The temporal degradation of bone collagen: A histochemical approach. Forensic Sci Int. 2014;240:104–110.
4. Pokines J, Symes SA, Roper C. Manual of Forensic Taphonomy. 1st ed. Baton Rouge: Taylor & Francis Group; 2013. p. 9–15.
5. Vass AA. The elusive universal post-mortem interval formula. Forensic Sci Int. 2011;204(1–3):34–40.
6. De-Giorgio F, Grassi S, d'Aloja E, Pascali VL. Post-mortem ocular changes and time since death: Scoping review and future perspective. Leg Med (Tokyo). 2021;50:101805.
7. Megyesi MS, Nawrocki SP, Haskell NH. Using accumulated degree-days to estimate the postmortem interval from decomposed human remains. J Forensic Sci. 2005;50(3):1–9.
8. Heaton V. Predicting the postmortem submersion interval for human remains recovered from U.K. waterways. J Forensic Sci. 2010;55(2):302–307.
9. Zhou C, Gilbert JD, Byard RW. Early diagnosis of Armanni–Ebstein phenomenon at autopsy. Forensic Sci Med Pathol. 2010;6(2):133–134.
10. Anderson GS, Bell LS. Deep coastal marine taphonomy: Investigation into carcass decomposition in the Saanich Inlet, British Columbia, using a baited camera. PLoS One. 2014;9(10).
11. Dell'Aquila M, De Matteis A, Scatena A, Costantino A, Camporeale MC, De Filippis A. Estimation of the time of death: Where we are now? Clin Ter. 2021;172:109–112.
12. Zissler A, Pittner S, Ehrenfellner B, Monticelli FC. Connective tissue degradation and collagen breakdown as late-stage markers in decomposition. Forensic Sci Res. 2021;6(3):183–193.
13. Scrivano S, Sanavio M, Tozzo P, Caenazzo L. Analysis of RNA in the estimation of post-mortem interval: A review of current evidence. Int J Legal Med. 2019;133:1629–1640.
14. Donaldson AE, Lamont IL. Estimation of post-mortem interval using biochemical markers. Aust J Forensic Sci. 2014;46:8–26.
15. Haas C, Neubauer J, Salzmann AP, Hanson E, Ballantyne J. Forensic transcriptome analysis using massively parallel sequencing. Forensic Sci Int Genet. 2021;52:102486.

16. Tozzo P, Scrivano S, Sanavio M, Caenazzo L. The role of DNA degradation in the estimation of post-mortem interval: A systematic review of the current literature. Int J Mol Sci. 2020;21:3540.
17. Pittner S, Ehrenfellner B, Monticelli FC, Zissler A, Sänger AM, Stoiber W, *et al.* Postmortem muscle protein degradation in humans as a tool for PMI delimitation. Int J Legal Med. 2016;130:1547–1555.
18. Fais P, Mazzotti MC, Teti G, Boscolo-Berto R, Pelotti S, Falconi M. HIF1α protein and mRNA expression as a new marker for post mortem interval estimation in human gingival tissue. J Anat. 2018;232:1031–1037.
19. Sampaio-Silva F, Magalhães T, Carvalho F, Dinis-Oliveira RJ, Silvestre R. Profiling of RNA degradation for estimation of post mortem interval. PLoS One. 2013;8(2):e56507.
20. Bell LS. Histotaphonomy. In: Crowder C, Stout S, editors. Bone Histology: An Anthropological Perspective. Boca Raton (FL): CRC Press; 2012. p. 241–251.
21. Jans MM. Microscopic destruction of bone. In: Pokines JT, Symes SA, editors. Manual of Forensic Taphonomy. Boca Raton (FL): CRC Press; 2013. p. 19–35.
22. Turner-Walker G, Jans MM. Reconstructing taphonomic histories using histological analysis. Palaeogeogr Palaeoclimatol Palaeoecol. 2008;266:227–235.
23. Mazzarini M, Falchi M, Bani D, Migliaccio AR. Evolution and new frontiers of histology in biomedical research. Microsc Res Tech. 2021;84(2):217–237.
24. O'Dowd G, Bell S, Wright S. Wheater's Functional Histology: A Text and Colour Atlas. Elsevier Health Sciences; 2023.
25. Byard RW, Winskog C. Histology in forensic practice: required or redundant? Forensic Sci Med Pathol. 2012;8(1):56–57.
26. Dettmeyer RB. Forensic Histopathology: Fundamentals and Perspectives. Springer; 2018.
27. Lau G, Lai SH. Forensic histopathology. Forensic Pathol Rev. 2008;5:239–265.
28. De La Grandmaison GL, Charlier P, Durigon M. Usefulness of systematic histological examination in routine forensic autopsy. J Forensic Sci. 2010;55(1):85–88.
29. Chan JK. The wonderful colors of the hematoxylin–eosin stain in diagnostic surgical pathology. Int J Surg Pathol. 2014;22(1):12–32.
30. Mishra NS, Wanjari SP, Parwani RN, Wanjari PV, Kaothalker SP. Assessment of collagen and elastic fibres in various stages of oral submucous fibrosis using Masson's trichrome, Verhoeff van Gieson, and picrosirius staining under light and polarizing microscopy. Journal of Dental Specialties. 2015;3(2):170–175.
31. Madea B, editor. Estimation of the time since death. 4th ed. Boca Raton (FL): CRC Press; 2023. doi:10.1201/9781003244974.
32. Zissler A, Stoiber W, Steinbacher P, Geissenberger J, Monticelli FC, Pittner S. Postmortem muscle protein degradation in humans as a tool for PMI estimation. Int J Legal Med. 2020;134(4):1367–1379.
33. Madea B, Saukko P. Forensic Medicine. Boca Raton (FL): CRC Press; 2018. p. 45–62.
34. Palić T, Štiglić D, Marinović Z, Bžan A. Histomorphological evaluation of porcine lung and spleen architecture under physiological conditions. Vet Pathol. 2024;61(3):456–464.
35. Pittner S, Bugelli V, Benbow ME, Ehrenfellner B, Zissler A, Campobasso CP, *et al*. Histological and molecular study of tissue decomposition and bacterial colonization for postmortem interval estimation. Forensic Sci Int. 2020;314:110418.
36. Sluis LV, Jones C, Henssge C. Histological indicators of early autolysis and putrefaction in internal organs: A comparative study for PMI estimation. J Forensic Leg Med. 2023;101:102021.
37. Almulhim HA. Time-dependent postmortem histological and biochemical alterations in rat organs for estimating postmortem interval. Forensic Sci Int. 2023;349:111608.
38. Jellinghaus K, Zissler A, Steinbacher P, Monticelli FC, Pittner S. Postmortem alterations of collagen and connective tissue structures in human muscle during decomposition. Int J Legal Med. 2018;132(5):1375–1383.
39. Garcés-Parra J, Rodríguez-Cuenca A, Pérez-Martínez M, Morales-García A. Late-stage histological degradation and liquefaction in postmortem soft tissues: Implications for PMI estimation. Forensic Sci Med Pathol. 2024;20(2):213–224.